

Broadband energy harvesting using acoustic black hole structural tailoring

This content has been downloaded from IOPscience. Please scroll down to see the full text.

2014 Smart Mater. Struct. 23 065021

(<http://iopscience.iop.org/0964-1726/23/6/065021>)

View [the table of contents for this issue](#), or go to the [journal homepage](#) for more

Download details:

IP Address: 147.188.128.74

This content was downloaded on 11/11/2014 at 20:21

Please note that [terms and conditions apply](#).

Broadband energy harvesting using acoustic black hole structural tailoring

Liuxian Zhao¹, Stephen C Conlon² and Fabio Semperlotti¹

¹Department of Aerospace and Mechanical Engineering, University of Notre Dame, Notre Dame, IN 46556, USA

²Applied Research Laboratory, The Pennsylvania State University, University Park, PA 16802, USA

E-mail: fsemperl@nd.edu

Received 29 October 2013, revised 25 March 2014

Accepted for publication 4 April 2014

Published 7 May 2014

Abstract

This paper explores the concept of an acoustic black hole (ABH) as a main design framework for performing dynamic structural tailoring of mechanical systems for vibration energy harvesting applications. The ABH is an integral feature embedded in the host structure that allows for a smooth reduction of the phase velocity, theoretically approaching zero, while minimizing the reflected energy. This mechanism results in structural areas with high energy density that can be effectively exploited to develop enhanced vibration-based energy harvesting. Fully coupled electro-mechanical models of an ABH tapered structure with surface mounted piezo-transducers are developed to numerically simulate the response of the system to both steady state and transient excitations. The design performances are numerically evaluated using structural intensity data as well as the instantaneous voltage/power and energy output produced by the piezo-transducer network. Results show that the dynamically tailored structural design enables a drastic increase in the harvested energy as compared to traditional structures, both under steady state and transient excitation conditions.

Keywords: energy harvesting, acoustic black hole, structural tailoring

(Some figures may appear in colour only in the online journal)

1. Introduction

Many applications in the aerospace, mechanical, and civil engineering fields have seen a large increase in the use of embedded electronics including, but not limited to, those used in vibration and noise control, structural health monitoring systems, and other types of smart structures. Such systems typically require continuous low input power [1], which is compatible with the performance of energy harvesting systems. This has been one of the contributing factors to the sudden growth in interest and research efforts dedicated to the development of energy harvesters powered by operational vibrations. To date, many different types of devices have been developed in order to harvest the energy associated with operational vibrations. Cantilever unimorphs [2] and bimorphs [3, 4], proof mass systems [5] and electromagnetic enhanced designs [6] are only a few examples of linear, resonance-based mechanisms developed to convert structure borne vibrations into storable electrical energy. Despite the

actual mechanism exploited to build the harvesting device, the majority of the linear resonance-based harvesters exhibit satisfactory performance only when the frequency of the external excitation matches the resonance frequency of the device. In fact, one of the major limitations of these harvesters is their narrowband performance. Structural and environmental vibrations are typically broadband so that the usable energy is effectively distributed over a wide frequency spectrum and spatial extent. In most cases, the distribution of this spectral energy cannot be predicted, prohibiting optimization of the harvester for specific frequency bands with high energy content. Interest in extending the frequency performance of the harvesters as well as reducing the dependence on the driving frequency has led to investigations of multimodal [7] and tunable [8, 9] devices and, later on, nonlinear mechanisms.

During the last decade, a variety of harvesters were developed by exploiting either one or a combination of these mechanisms [10]. In particular, nonlinear [11, 12] devices

have attracted considerable interest due to their ability to provide increased frequency performance. In the case of monostable devices [13], the nonlinear nature of the system allows locking into limit cycle vibrations for a wide range of driving frequencies, thereby extending their operating range. Despite the improved bandwidth, these devices exhibit tuning and stability issues during practical operating conditions. Bistable devices [14] have provided a way to alleviate some of these limitations and to extend the operating range even to stochastic input. However, they might require additional active devices to lock them into nonlinear motion under certain driving conditions. In addition to these limitations, it is observed that current harvesters, both linear and nonlinear, exhibit extremely limited performance under transient excitation conditions. In fact, the majority of harvesting devices are designed to operate at steady state and do not allow for an efficient energy conversion of transient signals. Although the spectral energy density for structure borne vibration decreases in the high frequency range, the potential for harvesting transient vibrations is of importance for developing devices based on environmentally discontinuous sources. In an effort to address these limitations of vibration-based energy harvesting, we explore a novel concept of structural design where the host structure becomes an effective component of the harvesting system.

The concept is based on the idea of tailoring the dynamics of the host structure by using embedded acoustic black holes (ABHs). The ABH can be seen as the acoustic counterpart of the well-known concept of a black hole in optics, which is an object from which light cannot escape. The ABH is an integral feature obtained by properly tailoring the local stiffness of the supporting structure. The gradual stiffness reduction results in a smooth decrease of the phase (and group) velocity of the elastic waves while minimizing the amplitude of reflected waves [15]. Under ideal conditions, which assume that the stiffness smoothly decreases to zero, the ABH will reduce the phase velocity to zero resulting in the so-called 'zero reflection' condition. When this condition is satisfied the reflection coefficient of the ABH is identically equal to zero. Another important effect that takes place when the thickness gradually decreases to zero is the progressive increase of the local wavenumber that eventually tends to infinity as the center of the ABH. In this paper, we will show how this wavenumber sweep mechanism is independent from the frequency of excitation and represents the key feature for achieving broadband energy harvesting.

The main physical principle exploited in the ABH was first observed by Pekeris [16] in 1946. He observed that the phase velocity of sound waves propagating in a stratified ocean progressively decreased to zero with decreasing depth. Many other researchers have predicted this effect for wave phenomena of a different physical nature (e.g. internal water waves in a horizontally inhomogeneous stratified fluid [17], particle scattering in quasi-classical quantum mechanics [18], etc). This concept was later extended to wave propagation in structures by Mironov [19]. He derived the wavenumber and the characteristic velocities of flexural waves in a thin plate with thickness decreasing smoothly to zero. He also showed

that the reflection coefficient can become quite large, quickly converging to one, in the presence of a small but non-zero residual thickness. Later, Krylov [20, 21] showed that the deposition of absorbing thin layers on the surface of the ABH can greatly reduce these reflections in the non-ideal case (i.e. non-zero residual thickness).

In this paper, we investigate the use of ABHs to design dynamically tailored structures for enhanced vibration energy harvesting under both steady state and transient excitation. In particular, we will show how the wave propagation characteristics provided by embedded ABH features result in (1) localized structural areas with high energy density and (2) broadband energy absorption that is a direct consequence of the wavenumber sweep mechanism produced by the ABH.

2. Theoretical background

The fundamental operating principle of the ABH is based on the concept of the 'zero reflection' effect which takes place when the phase velocity progressively decreases to zero with the propagating distance [19, 22]. This concept can be illustrated by exploring the propagation characteristics of flexural waves in a two-dimensional plate terminated by a tapered edge. The edge profile (figures 1(a) and (b)) is described by a power-law relation of the form $h(x) = \epsilon x^m$, where m is a rational number greater than 2 and ϵ is a constant.

As a wave propagates through the tapered profile towards the edge, the complex amplitude $W(x)$ of the wave [23] can be expressed as follows:

$$W(x) = B(x) \exp(j\theta(x)) \quad (1)$$

where $B(x)$ is the amplitude of the wave at the location x , j is the imaginary unit, and $\theta(x) = \int_0^x k(x)dx$ is the total accumulated phase. If the thickness of the plate varies along the propagation direction, i.e. $h=f(x)$, where f is an arbitrary continuous function, then the wavenumber also becomes a function of the spatial coordinate $k=g(x)$. The dynamic response of a thin plate with varying thickness is described by [24]:

$$\begin{aligned} D\nabla\nabla w + 2\frac{\partial D}{\partial x}\frac{\partial}{\partial x}\nabla w + 2\frac{\partial D}{\partial y}\frac{\partial}{\partial y}\nabla w + \nabla D\nabla w \\ - (1-\nu)\left(\frac{\partial^2 D}{\partial x^2}\frac{\partial^2 w}{\partial y^2} - 2\frac{\partial^2 D}{\partial x\partial y}\frac{\partial^2 w}{\partial x\partial y} + \frac{\partial^2 D}{\partial y^2}\frac{\partial^2 w}{\partial x^2}\right) \\ = \rho h\frac{\partial^2 w}{\partial t^2} \end{aligned} \quad (2)$$

where $D = Eh^3/12(1-\nu^2)$ is the bending stiffness, E is the Young's modulus, ν is the Poisson's ratio, ρ is the density, h is the thickness of the plate, x and y are the spatial coordinates and t is the time variable. Assuming the thickness is varying according to the power law $h(x) = \epsilon x^m$ and assuming plane wave-like solutions as in equation (1), the flexural

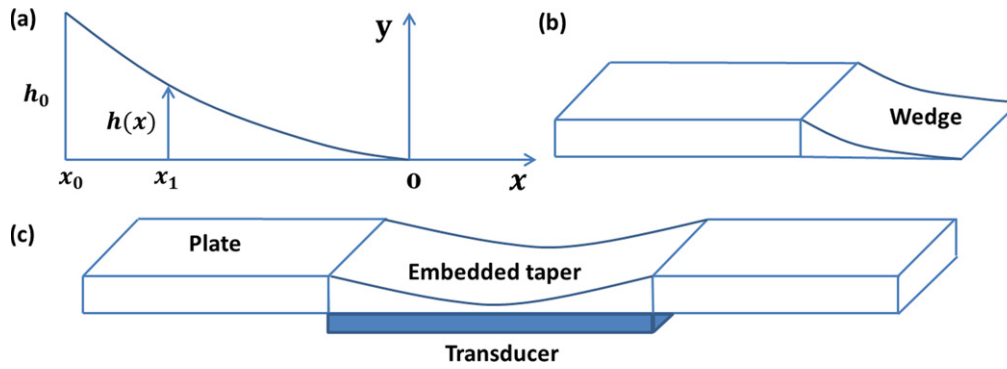


Figure 1. Schematic of the tapered edge according to a power-law profile. (a) 2D profile of a smooth tapered wedge, (b) 3D schematic of a thin plate terminated by a tapered edge, (c) 3D schematic of a thin plate with a tapered embedded section. The schematic also shows the possible application of a surface mounted piezo-transducer on the tapered area.

wavenumber is given by:

$$k(x) = \sqrt[4]{12} \sqrt{\frac{k_l}{\epsilon x^m}} \quad (3)$$

where k_l is the longitudinal wavenumber in a thin plate of constant thickness, which is defined as $k_l^2 = \frac{\rho(1-\nu^2)\omega^2}{E}$.

In such a structure, the phase and group velocities are given by [19]:

$$\begin{aligned} c_p &= \sqrt[4]{\frac{E}{12\rho(1-\nu^2)}} \sqrt{\omega \cdot \epsilon x^m} \\ c_g &= \sqrt[4]{\frac{4E}{3\rho(1-\nu^2)}} \sqrt{\omega \cdot \epsilon x^m} \end{aligned} \quad (4)$$

where ω is the angular frequency of the propagating wave.

The propagation time T of a wave packet propagating from an initial cross section $x = x_0$ to $x = x_1$ is:

$$T = \int_{x_0}^{x_1} \frac{dx}{c_g} = \sqrt[4]{\frac{12\rho(1-\nu^2)}{E(\epsilon\omega)^2}} \frac{1}{2-m} (x_1^{1-m/2} - x_0^{1-m/2}) \quad (5)$$

If $m \geq 2$ and x_1 tends to zero, both the phase and the group velocity tend to zero and the time of flight of the wave tends to infinity; therefore the wave will never reach the tip of the wedge. Also, if $m \geq 2$ the phase $\theta(x)$ goes to infinity [18], meaning that the edge of the plate becomes a point of singularity where the particle displacement goes to infinity. It should be noted that, in practice, the thickness cannot be made zero due to fabrication limitations (nor would this be a desired condition for practical structures). For the sake of completeness, we also observe that the taper exponent m must also satisfy the smoothness condition [18]. This residual thickness has important implications for the performance of the ABH. In the case of a thin plate terminated by a tapered wedge (figure 1(b)), the residual thickness at the truncation point gives rise to reflected waves that can drastically reduce the black hole effect. Assuming a non-zero loss factor for the host structure, the coefficient of reflection can be related to the

cutoff thickness h_1 by the following relation [19]:

$$R = \exp\left(-2 \int_{x_0}^{x_1} \text{Im } k(x) dx\right) \quad (6)$$

In metallic materials, such as aluminum, even in the case of small residual thickness h_1 the coefficient of reflection R can be about 50–70%. We observe that in the limit case of zero damping, $\text{Im}(k) \rightarrow 0$ and $R \rightarrow 1$. Similarly, in case of an embedded ABH (figure 1(c)) the same considerations would hold for the energy transmitted through the taper.

Using a one-dimensional analysis and assuming plane harmonic waves, the time-averaged energy density is given by:

$$\begin{aligned} \langle P(x) \rangle &= \langle U(x) \rangle + \langle T(x) \rangle = \frac{1}{2T} \int_t^{t+T} E \left(\frac{\partial W}{\partial x} \right)^2 dt \\ &+ \frac{1}{2T} \int_t^{t+T} \rho \dot{W}^2 dt = 1/2 \rho \omega^2 B^2(x) \end{aligned} \quad (7)$$

where P is the total energy density, U is the strain energy density and T is the kinetic energy density, $\langle \rangle$ is the time average over a period, ρ is the material density, ω is the frequency of the harmonic wave and B is the displacement amplitude of the wave. Note that the total energy depends on the spatial coordinate via the wave amplitude and tends to infinity as the wave approaches the point of zero thickness. Therefore, theoretically the center of the ABH is also a singularity point with respect to the energy density.

From equation (3) it can be seen that as the wave travels through the tapered area approaching the theoretical zero thickness (that is, as x tends to zero) the wavenumber progressively approaches infinity or, equivalently, the wavelength approaches zero. Note that this progressive variation of the wavelength with the propagation distance, referred to as a ‘wavelength sweep’, is purely passive and occurs *regardless of the initial wavelength* of the incident wave. This aspect is of crucial importance in determining the broadband characteristics of the ABH tapered structure. In fact, in piezoelectric-based vibration energy harvesting maximum performance (that is, maximum converted energy) is obtained when the wavelength of the excitation matches the optimal wavelength corresponding to the resonance frequency of the piezo-

transducer. In conventional (non-tapered) structures, this condition results in energy being effectively harvested in only a very narrow band around the tuning frequency of the piezo. In ABH tapered structures, all the wavelength components entering the ABH are progressively compressed to zero following a continuous wavelength sweep that forces every incoming wave through the resonance condition of the transducer. This mechanism makes the ABH a passive adaptive structural element, able to compress virtually any incoming wavelengths.

Although the present study does not address the design optimization of ABH tapered structures, the following consideration should be carefully evaluated for the problem at hand. In order to maximize the broadband characteristics of the ABH energy harvesting, the resonance condition of the piezo should be designed to occur at the lower limit of the wavelength. We observe that the ABH effectively acts as a broadband energy focusing lens with the focal point located at the center of the ABH.

3. ABHs for piezoelectric-based energy harvesting

We have shown theoretically that embedded ABHs result in structural areas with a high (ideally infinite) level of energy density and produce a wavelength sweep via a completely passive mechanism. These two features can be of great practical interest for piezoelectric energy harvesting. In particular, the existence of structural areas behaving as effective energy sinks can be exploited to identify *a priori* the optimal locations of the piezo-transducers. Also, as the wave travels through the tapered ABH area it undergoes a wavelength sweep (from larger to smaller wavelengths) that can be exploited as a passive adaptive mechanism to tune an incoming signal to the optimal operating conditions of the transducer (e.g. its resonance frequency). These characteristics suggest that placing the transducers at the ABH locations should allow for considerably more efficient energy harvesting regardless of the excitation conditions. To explore the concept of energy harvesting enhancement via dynamic structural tailoring we have developed fully coupled electro-mechanical models of an ABH tapered plate with surface mounted piezo-transducers (figure 1(c)). Each transducer is shunted on a lumped resistor in order to simulate the resistive load produced by the harvester electronics and energy storage mechanism. The finite element (FE) model is used to explore the response of the system to either steady state or transient loads.

4. Numerical modeling of the ABH tapered structure

4.1. Effect of the ABH on incident waves

As previously shown theoretically, the phase and group velocities decrease when the propagating wave interacts with the ABH. In the limit case, this mechanism results in infinite particle displacement, thus infinite energy density, at the center of the ABH. In order to study the behavior of

propagating waves when interacting with the ABH, a 2D tapered plate model (1000 mm × 8 mm) with a single centered ABH of length $l_h = 100$ mm was developed (figure 2(a)). The model was used to calculate the transient response of the structure to a 2.5-period Hanning-windowed tone burst with two different center frequencies, $f_{c1} = 100$ kHz and $f_{c2} = 5$ kHz. The structural damping η was set to zero in order to clearly isolate the effect of the ABH on the vibrational energy. The FE models was assembled and solved using the commercial finite element analysis package Ansys [25]. The 2D plate was simulated using 8-noded plane elements under plane stress conditions. A comprehensive list of the material properties used in the FE model is provided in table 1.

The transient response of the structure at the two different frequencies is provided in figures 2(b) and (c) in terms of time–space data. Both plots clearly show the characteristic lines indicating the propagating waves. The difference in slope of the characteristic lines highlight the higher phase velocity of the high frequency component. As the high frequency wave travels through the ABH the wavefronts decrease in speed (as shown by the change in the local slope; figure 2(b), red dotted circle) due to the effect of the taper. Nevertheless, due to the higher initial speed the majority of the wave can still propagate through the ABH. When the frequency of the initial wave packet is reduced to $f_{c2} = 5$ kHz, the lower initial velocity allows a substantial reduction of the phase velocity so that part of the wave is effectively trapped inside the ABH. Note that in the absence of material loss factor or any dissipative mechanism, the wave still travels forward but at a considerably lower phase velocity. These results also confirm that, as expected, the finite size of the ABH introduces physical bounds in the range of wavelengths that can effectively be controlled.

Frequency-wavenumber analysis was also performed (using a 2D Fourier transform approach) in order to explore the effect of the ABH on the spectral content of the propagating signal. Results are shown in figure 3 for the excitation case at $f_{c2} = 5$ kHz. In particular, figure 3(b) shows the frequency wavenumber on the constant thickness sections 1 and 3. Given the input tone burst, the corresponding propagating waves have a wavenumber ranging from $k_f = 40$ to 60 rad m^{-1} . Some wavenumber components outside this range are also visible, although these are mostly low amplitude signals corresponding to dispersed waves escaping the ABH. Figure 3(c) shows the frequency-wavenumber analysis of the ABH section 2. In agreement with the analytical formulation, numerical results indicate that in the ABH area the wave undergoes a continuous wavenumber (or equivalently, wavelength) sweep due to the tapered profile. These results support the previous observation that the ABH acts as a fully passive mechanism for wave tuning.

4.2. Energy harvesting in ABH dynamically tailored plates

Two different models were developed to numerically investigate the energy harvesting performance of the ABH tapered structure: (1) a flat plate (constant thickness) model and (2) a tapered plate with embedded ABHs. Both plates were made

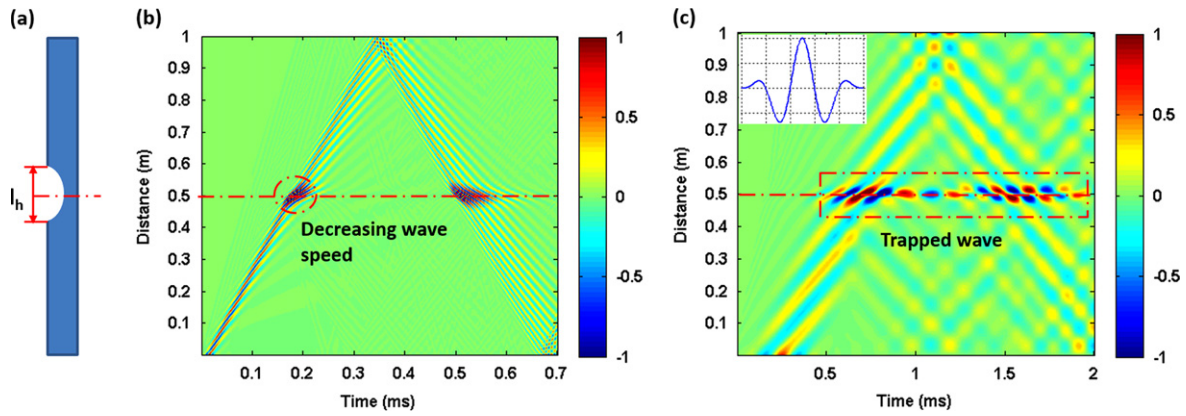


Figure 2. Time–space analysis of a tapered plate with a single embedded ABH. (a) A schematic model of the tapered plate. (b) and (c) The time–space results of the response of the plate to a tone burst excitation with center frequency of $f_{c1} = 100$ kHz and $f_{c2} = 5$ kHz, respectively. The color bars show the normalized wave amplitude.

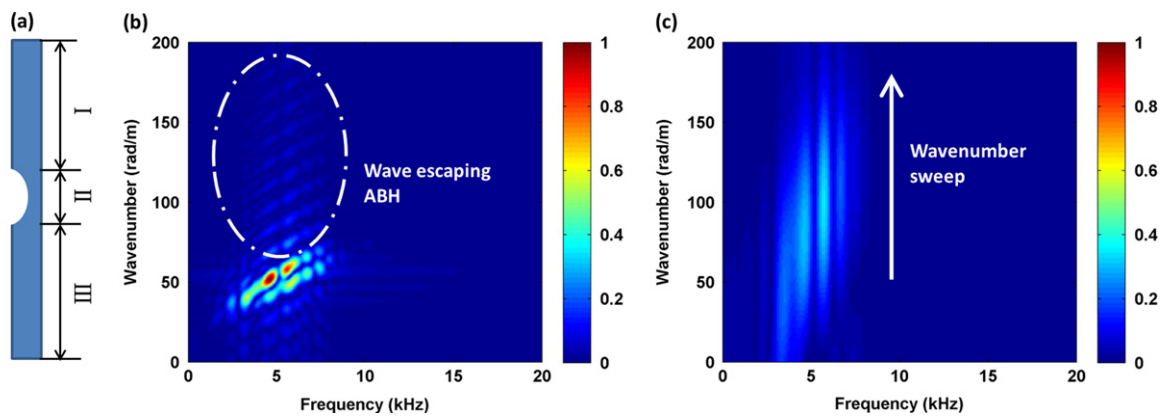


Figure 3. Frequency-wavenumber analysis of the tapered plate with a single embedded ABH excited by a tone burst at $f_{c2} = 5$ kHz. (a) A schematic model of the tapered plate. (b) and (c) The frequency-wavenumber results for the flat (I and III) and tapered section 2 of the plate, respectively.

Table 1. Summary of the material properties of the aluminum plate and the piezo-transducer.

Aluminum	
Young's Modulus (GPa): E	79
Poisson Ratio: ν	0.33
Density (kg m^{-3}): ρ	2700
Structural damping: η	0
Piezoelectric material: PZT-5H	
Young's modulus (GPa)	
E_{11}	62
E_{33}	50
Poisson's ratio: ν	0.3
Density (kg m^{-3}): ρ	7800
Piezoelectric constants ($\times 10^{-12}$ m volt $^{-1}$)	
d_{33}	650
d_{31}	-320
Coupling coefficients	
k_{33}	0.75
k_{31}	0.44
Relative dielectric constant: ϵ_{33}	3800
Structural damping: η	0

out of aluminum with dimensions $1700 \text{ mm} \times 8 \text{ mm}$. The flat plate was used as reference model to evaluate the performance of the structural tailoring approach. The tapered plate consisted of five ABHs having a power law profile with the following parameters: $\epsilon = 5$ and $m = 2.2$. Each hole had a length $l_h = 100$ mm and consecutive holes were equally spaced $l_s = 140$ mm from center to center. We observe that, in this study, the choice of the ABH design parameters was not optimized for maximum performance. It is envisioned that the taper coefficient ϵ and the exponent m can be selected following an optimization analysis to maximize the amount of energy harvested. Five unimorph piezo-transducers with length $l_T = 100$ mm were attached to the flat side of the plate in correspondence to each ABH, as shown in figure 4. The transducers are made of PZT-5H polarized in the d_{31} direction [26]. This coupling was selected because it is particularly efficient at coupling the electrical response of the transducer with flexural vibrations (which dominated the response of the structural system under study). The nodes between the piezo-transducer and the plate are merged together, which accounts for full compatibility of the strains. The voltage degree of freedom of the nodes on the top and bottom surfaces of the transducers are coupled together to simulate the electrodes.

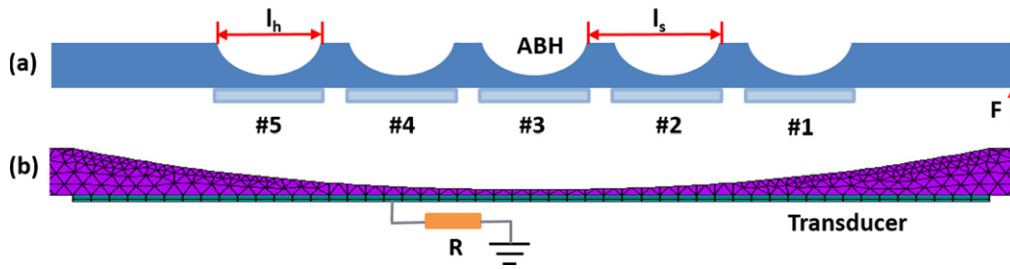


Figure 4. (a) A schematic of the 2D tapered plate with five embedded and equally spaced ABHs used for the numerical simulations, and (b) a detailed view of the FE model around one of the ABH features showing the power law profile and the surface mounted piezo-transducer.

The voltage at the top electrode is set to zero to simulate the ground [27, 28].

An external lumped resistor was also connected to each piezo-transducer in order to simulate the resistive load produced by the harvester electronics. The relationships between the output voltage of the transducer and the input to the resistive load are [29]:

$$\begin{aligned} V_p(t) &= V_R(t) \\ I_R(t) &= \omega Q_p(t) \end{aligned} \quad (8)$$

where V_p is the output voltage from the transducer, V_R is the voltage across the resistor load, I_R is the current through the resistive load, and Q_p is the electric charge on the electrodes of the transducer.

The FE models were assembled and solved using the commercial finite element analysis package Ansys. The 2D plates were simulated using 8-noded plane elements under plane stress conditions. The surface mounted transducers were simulated using 8-noded plane elements with piezoelectric capabilities while the external electric circuitry was simulated using a lumped resistor connected to the transducer.

4.2.1. Steady state analysis. The effect of the ABH dynamic tailoring on the energy harvesting performance of the piezo-transducers was initially investigated at steady state conditions. The tapered plate (figure 4(a)) was excited on the right-hand side using a force $F=100$ N sweeping the frequency band $f=0$ to 10 kHz. The external resistive load simulating the harvester electronics was set to $R=1 \Omega$. We highlight that such a low value of the resistance was intentionally selected in order to minimize the damping effect produced by the shunted piezo on the dynamic response of the plate. By minimizing the damping effect, differences between the dynamics of the flat and tapered plate can be easily correlated to the effect of the structural taper. Note that for practical implementation and optimal harvesting performance, different values of the resistor might be needed. Nevertheless, this assumption regarding the resistance value will not alter the qualitative behavior of the system and the main findings illustrated in the following numerical results.

The results of the numerical simulations are shown in figure 5(a) in terms of dissipated power spectra at a selected transducer. In order to compare the performance of the

different transducers between each other and across the two configurations, we introduce a relative index of performance represented by a non-dimensional normalized energy ratio $E_r = E_o^{(n)} / (E_i \max_n \{E_o^{(n)} / E_i\})$, where $E_o^{(n)}$ is the dissipated energy on the resistor connected to the n th transducer and E_i is the mechanical input energy, respectively. Note that, according to the definition of this index, a unit value of E_r indicates that the corresponding transducer was selected for reference (it does not indicate that 100% of the input energy is being absorbed). The energy ratio E_r at each transducer is shown in figure 5(b). The energy ratio is used as a metric to estimate the amount of mechanical energy extracted by the system via the piezo-transducers, which is the energy that could potentially be converted and harvested. The power spectra indicate that, in the frequency range where the ABH interacts with the incoming waves (above 5 kHz), the harvested energy produced is drastically increased compared to the non-tapered structure. Also, the energy ratio in the range 5 to 10 kHz is also drastically increased. These results are consistent with the above analytical predictions suggesting that the ABH produces structural areas with high (theoretically infinite) energy density. Note that for the selected ABH geometry, $f=5$ kHz represents a cutoff frequency in terms of the efficiency of the ABH.

In order to gain additional insight into the effect of the ABHs, structural intensity (SI) was used as a metric to visualize the spatial distribution of the mechanical energy and to compare the tapered with the reference structure. SI is the mechanical power flow per unit cross-sectional area that, in a 2D plane structure, can be expressed as [30–32]:

$$\begin{aligned} I_x &= -\frac{1}{2} \operatorname{Re} (\sigma_x v_x^* + \tau_{xy} v_y^*) \\ I_y &= -\frac{1}{2} \operatorname{Re} (\sigma_y v_y^* + \tau_{yx} v_x^*) \\ \bar{I} &= I_x \hat{i} + I_y \hat{j} \end{aligned} \quad (9)$$

where σ_x and σ_y are the complex stresses in the x and y directions, τ_{xy} is complex shear stress, v_x and v_y are the complex velocities in the x and y directions, Re indicates the real part, $*$ indicates the complex conjugate, \hat{i} and \hat{j} are unit vectors in the plane, I_x and I_y are the SI components in the x and y directions, and \bar{I} is the total SI.

According to equation (9), the SI was calculated for both the flat and tapered plates using the input from the 2D finite

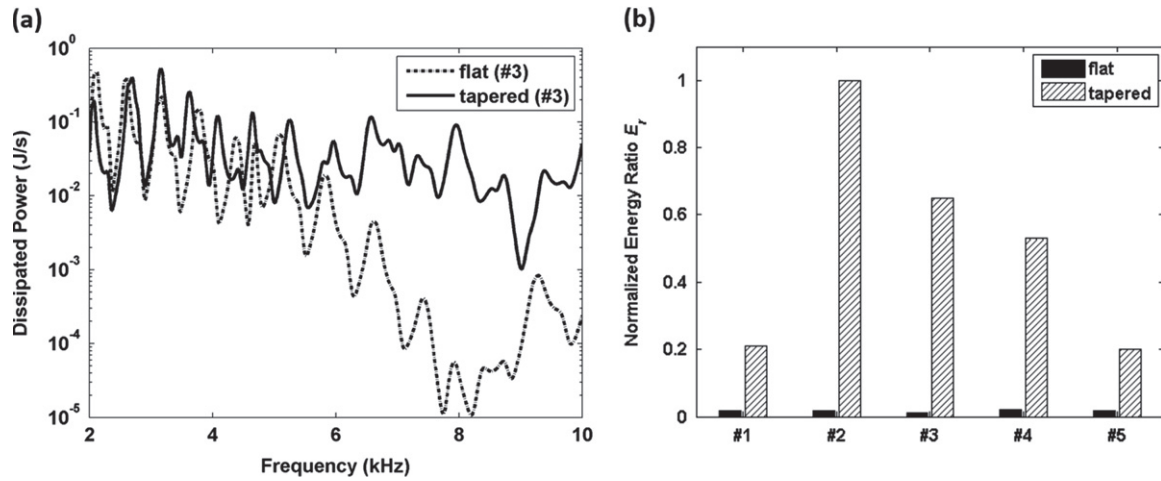


Figure 5. Numerical results showing the performance of the energy harvesting system under steady state excitation. (a) The comparison between the dissipated power spectra of the flat and tapered plate at transducer #3, and (b) the normalized energy ratio for each transducer in the 5 to 10 kHz frequency band. The direct comparison of the performance between the two structural configurations shows the drastic increase in the converted (i.e. extracted) energy due to the new dynamically tailored design.

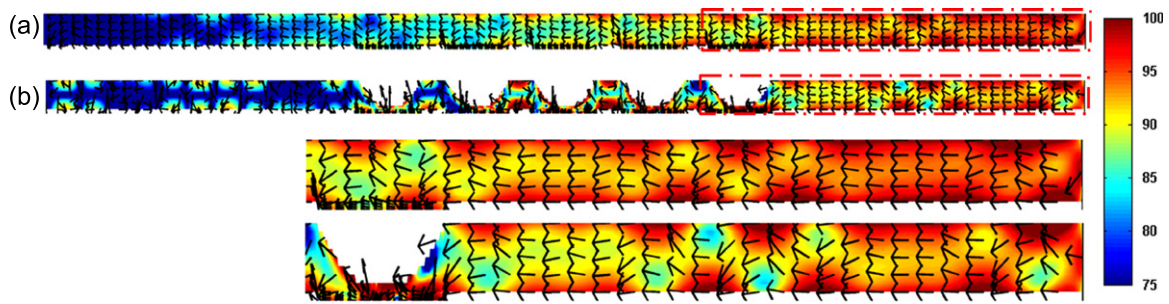


Figure 6. Structural intensity maps for the (a) flat and (b) tapered plates; (c) and (d) zoom-in into the right-end section (dashed red box). The color shows the SI level in dB while the arrows show the energy flow direction. Both structures are excited at the right-end side by a 5 kHz harmonic excitation while maintaining constant input power. The direct comparison shows that the energy flow is highly disrupted by the presence of the tapers and highly attenuated in the area downstream of the tapers.

element model discussed above. The stresses and velocity components were estimated using harmonic analysis. The resulting SI maps for the two structures (flat and tapered) with surface mounted transducers are shown in figures 6(a) and (b). The maps are expressed in dB scale and calculated at a frequency $f=5$ kHz while maintaining constant the input power between the two configurations. The distribution of SI indicates that the ABH strongly affects the mechanical energy by providing higher attenuation, particularly in the area downstream of the tapers. Figures 6(c) and (d) provide a detailed view of the intensity distribution in the initial section of the plates and of the first transducer.

To obtain a more quantitative estimate of the effects produced by the ABHs in terms of spatial energy distribution we introduce an absolute index of performance consisting in a non-dimensional attenuation coefficient and defined as follows:

$$\begin{aligned} \alpha_f &= (I_r - I_f) / I_r \\ \alpha_t &= (I_r - I_t) / I_r \end{aligned} \quad (10)$$

where α_f and α_t are the attenuation coefficients of the flat and tapered plates with external circuitry, I_f and I_t are the

structural intensity of the flat and tapered plates with external electrical circuitry, and I_r is the reference structural intensity of the flat plate without external electrical circuitry. This coefficient is intended to complement the information provided by the non-dimensional energy index E_r by providing an estimate of the overall effect that the transducer network has on the host structure. According to equation (10), higher values of the index α indicate a stronger attenuation of the vibrational energy. Observing that the only source of energy dissipation is represented by the external electric resistors (no structural damping is added to the host structure nor to the transducers), and thus that energy can only be extracted via the transducers at the ABH locations, the attenuation index becomes a direct indicator of the efficiency of the energy absorption mechanism in ABH tapered structures. The distribution of the normalized (with respect to $\max |\alpha_i|$) attenuation coefficients for both the flat and the tapered plate is shown in figure 7. A direct comparison of the attenuation coefficient maps clearly show that the energy attenuation in the tapered plate is about 50–60% higher than in the corresponding flat plate. Note that large energy attenuation is particularly visible at the transducer locations,

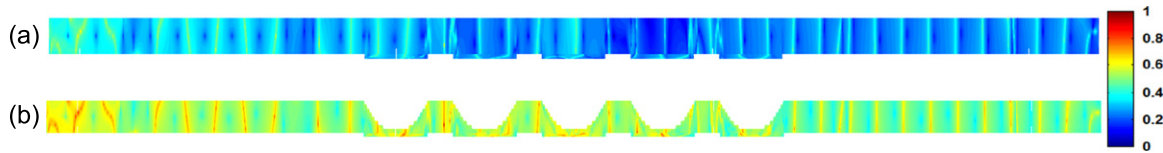


Figure 7. Maps of the normalized attenuation index α for the (a) flat and (b) tapered plates. The attenuation levels indicate that the tapered structure allows a more effective energy extraction mechanism leading to an increase in the attenuation coefficients up to 60%.

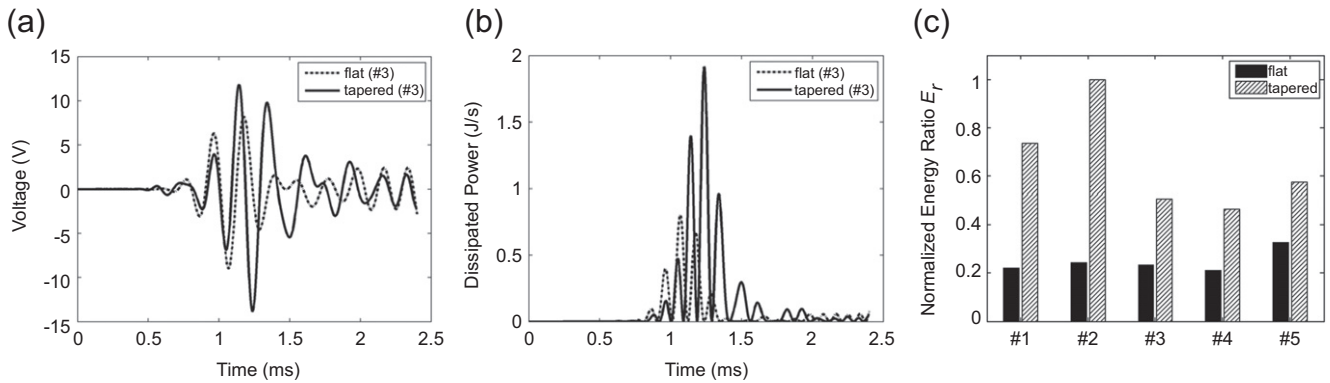


Figure 8. Numerical results showing the performance of the energy harvesting system under transient excitation for the two structural configurations. (a) The instantaneous output voltage from transducer #3; (b) the corresponding output power spectra; (c) a comparison of the energy ratio from the five transducers. Results show that the amount of energy absorbed from the piezo-transducers undergoes a drastic increase up to 80%.

thereby confirming the increased energy absorption effect produced by the taper.

4.2.2. Transient analysis. The performances of the ABH-based dynamic tailoring were also tested under transient excitation. For this test case, the structure was excited by a Hanning-windowed tone burst force with a center frequency $f = 5$ kHz and an amplitude $F = 100$ N applied at the right end of the plate. The response of the two systems (figure 8) was quantified in terms of instantaneous voltage and dissipated power at the transducer #3, and calculating the normalized energy ratio for each transducer. As previously discussed, when the wave packet travels through the ABH its phase velocity decreases so that the wave is partially or completely trapped in the ABH. During this process the wavelengths contained in the wave packet are progressively compressed to zero regardless of their initial value. When the local wavelength matches the resonance frequency of the piezo-transducer the vibrational energy is efficiently absorbed and converted into electrical energy. The first antisymmetric resonance frequency [33] of the piezo-transducer can be calculated according to $f^A = c/2l_T$, where c is the bulk longitudinal wave speed in the piezoelectric material. For the selected transducer configuration $f^A = 17.9$ kHz. We observe that the wavelength corresponding to f^A is the optimal value λ_{opt} at which the efficiency of the piezoelectric conversion is maximized. By exciting the flat plate structure at a frequency $f = 5$ kHz, the characteristic wavelength of the propagating waves is larger than λ_{opt} , thereby reducing the efficiency of the conversion mechanism. On the contrary, in a tapered plate the waves undergo a continuous wavelength

sweep inside the ABH, resulting in a continuous reduction of the wavelength that eventually will match the optimal wavelength of the transducer λ_{opt} . When this condition is met, the transducer delivers high energy absorption and conversion efficiency.

Numerical results confirm that this mechanism is able to provide a drastic increase in both the instantaneous voltage/power produced by the transducers and in the normalized energy ratio. In particular, the energy ratios show an increase in energy harvested up to 80%.

Note that these results were obtained for a tone burst with a 5 kHz center frequency that corresponds to the low cutoff frequency for the selected ABH geometry. This means that the estimated increase in the harvesting efficiency under transient excitation should be considered as a lower bound for the performance of the design.

5. Conclusions

In this paper, we presented a theoretical and numerical study investigating the concept of dynamic structural tailoring for vibration-based energy harvesting applications. The structural dynamic tailoring is implemented using the concept of embedded acoustic black holes (ABH). The embedded ABH produces structural areas with high energy density (theoretically approaching infinity) where the incident wave undergoes a continuous wavelength sweep due to a purely passive mechanism. These two characteristics provide a viable and effective approach to solving two important limitations of current vibration-based energy harvesting systems, which is the identification of the transducer location for optimal

absorption and increased efficiency in the presence of broadband excitation. Fully coupled electro-mechanical finite element models were developed to numerically investigate the performance of the ABH based design. Numerical results showed that the new design can drastically increase the efficiency of the energy absorption mechanism during both steady state and transient excitation. The transient excitation greatly benefits from the wavelength sweep mechanism occurring in the ABH tapered area. In particular, the wavelength sweep allows the effective absorption and conversion of mechanical energy from frequency bands corresponding to wavelengths of the incident signal which are much larger than the optimal wavelength of the piezo-transducer.

References

- [1] Badel A, Richard C and Guyomar D 2005 Piezoelectric energy harvesting device optimization by synchronous electric charge extraction *J. Intell. Mater. Syst. Struct.* **16** 865–76
- [2] Abdelkefi A, Najjar F, Nayfeh A H and Ayed S B 2011 An energy harvester using piezoelectric cantilever beams undergoing coupled bending-torsion vibrations *Smart Mater. Struct.* **20** 115007
- [3] Zhang L, Williams K A and Xie Z 2011 Enhanced coupled field modeling of PZT cantilever bimorph energy harvester *Applied Mechanics and Materials* **145** 21–6
- [4] Rafique S and Bonello P 2010 Experimental validation of a distributed parameter piezoelectric bimorph cantilever energy harvester *Smart Mater. Struct.* **19** 1–15
- [5] Tang X and Zuo L 2011 Enhanced vibration energy harvesting using dual-mass systems *J. Sound Vib.* **330** 5199–209
- [6] Challa V R, Prasad M G and Fisher F T 2009 A coupled piezoelectric-electromagnetic energy harvesting technique for achieving increased power output through damping matching *Smart Mater. Struct.* **18** 095029
- [7] Tadesse Y, Zhang S and Priya S 2009 Multimodal energy harvesting system: piezoelectric and electromagnetic *J. Intell. Mater. Syst. Struct.* **20** 625–32
- [8] Harne RL 2012 Concurrent attenuation of, and energy harvesting from, surface vibrations: experimental verification and model validation *Smart Mater. Struct.* **21** 035016
- [9] Rafique S, Bonello P and Shuttleworth R 2013 Experimental validation of a novel smart electromechanical tuned mass damper beam device *J. Sound Vib.* **332** 4912–26
- [10] Basset P, Galayko D, Cottone F, Guillemet R, Blokhina E, Marty F and Bourouina T 2014 Electrostatic vibration energy harvester with combined effect of electrical nonlinearities and mechanical impact *J. Micromech. Microeng.* **24** 035001
- [11] Cottone F, Vocca H and Gammaitoni L 2009 Nonlinear energy harvesting *Phys. Rev. Lett.* **102** 080601
- [12] Hubbard S A, McFarland D M, Bergman L A and Vakakis A F 2010 Targeted energy transfer between a model flexible wing and nonlinear energy sink *J. Aircraft* **47** 1918–31
- [13] Zhao S and Erturk A 2013 On the stochastic excitation of monostable and bistable electroelastic power generators: relative advantages and tradeoffs in a physical system *Appl. Phys. Lett.* **102** 103902
- [14] Hame R L and Wang K W 2013 A review of the recent research on vibration energy harvesting via bistable systems *Smart Mater. Struct.* **22** 023001
- [15] Mironov M A and Pislyakov V V 2002 One-dimensional acoustic waves in retarding structures with propagation velocity tending to zero *Acoust. Phys.* **48** 400–5
- [16] Pekeris C L 1946 Theory of propagation of sound in a half-space of variable sound velocity under conditions of formation of a shadow zone *J. Acoust. Soc. Am.* **18** 295–315
- [17] Badulin S I, Tsimring L S and Shrira V I 1983 Trapping and vertical focusing of internal waves in the pycnocline due to horizontal inhomogeneities of the stratification and currents *J. Fluid Mech.* **273** 459–63
- [18] Landau L D and Lifshits E M 1977 *Quantum Mechanics* (Oxford: Pergamon Press)
- [19] Mironov M A 1988 Propagation of a flexural wave in a plate whose thickness decreases smoothly to zero in a finite interval *Sov. Phys.—Acoust.* **34** 318–9
- [20] Krylov V V and Bowyer E P 2013 Acoustic black holes: a new approach to vibration damping in light-weight structures *Proc. Inst. Acoust.* **35** 184–91
- [21] Krylov V V and Tilman F J B S 2004 Acoustic ‘black hole’ for flexural waves as effective vibration dampers *J. Sound Vib.* **274** 605–19
- [22] Conlon S C, Semperlotti F and Fahnlone J B 2013 Passive control of vibration and sound transmission for vehicle structures via embedded acoustic black holes *INTER-NOISE and NOISE-CON Congr. and Conf. Proc. (Denver, CO)* vol 246 pp 176–84
- [23] Krylov V V 2004 New type of vibration dampers utilizing the effect of acoustic ‘black holes’ *Acta Acustica United With Acustica* **90** 830–7
- [24] Timoshenko S, Young D H and Weaver W 1974 *Vibration Problems in Engineering* (New York: Wiley)
- [25] ANSYS 14.5 Help Electromagnetic analysis guide
- [26] Kwok K W, Wang B, Chan H L W and Choy L 2002 Self-polarization in PZT films *Ferroelectrics* **271** 69–74
- [27] Liu W and Giurgiutiu V 2007 Finite element simulation of piezoelectric wafer active sensor for structural health monitoring with coupled-field elements *Proc. SPIE* **6529** 65293R
- [28] Yang J 2009 *Special Topics in the Theory of Piezoelectricity* (New York: Springer)
- [29] Zhu M, Worthington E and Njuguna J 2009 Coupled piezoelectric-circuit FEA to study influence of a resistive load on power output of piezoelectric energy devices *Proc. SPIE* **7362** 736202
- [30] Gavric L, Carlsson U and Feng L 1997 Measurement of structural intensity using a normal mode approach *J. Sound Vib.* **206** 87–101
- [31] Semperlotti F and Conlon S C 2010 Structural damage identification in plates via nonlinear structural intensity maps *J. Acoust. Soc. Am.* **127** EL48–53
- [32] Pavic G 1987 Structural surface intensity: an alternative approach in vibration analysis and diagnosis *J. Sound Vib.* **115** 405–22
- [33] Giurgiutiu V 2008 *Structural Health Monitoring with Piezoelectric Wafer Active Sensors* (New York: Academic)